Journal of Physics B: Atomic, Molecular and Optical Physics

PAPER

Adiabatic potentials of cesium $(nD_J)_2$ Rydberg–Rydberg macrodimers

To cite this article: Xiaoxuan Han *et al* 2019 *J. Phys. B: At. Mol. Opt. Phys.* **52** 135102

IOP Publishing Journal of Physics B: Atomic, Molecular and Optical Physics
J. Phys. B: At. Mol. Opt. Phys. **52** (2019) 135102 (10pp) https://doi.org/10.1088/1361-6455/ab1371

Adiabatic potentials of cesium $(nD_J)_2$ Rydberg–Rydberg macrodimers

Xiaoxuan Han[1,2], Suying Bai[1,2], Yuechun Jiao[1,2], Georg Raithel[1,3], Jianming Zhao[1,2] and Suotang Jia[1,2]

[1] State Key Laboratory of Quantum Optics and Quantum Optics Devices, Institute of Laser Spectroscopy, Shanxi University, Taiyuan 030006, People's Republic of China
[2] Collaborative Innovation Center of Extreme Optics, Shanxi University, Taiyuan 030006, People's Republic of China
[3] Department of Physics, University of Michigan, Ann Arbor, Michigan 48109-1120, United States of America

E-mail: zhaojm@sxu.edu.cn

Received 8 January 2019, revised 22 March 2019
Accepted for publication 26 March 2019
Published 18 June 2019

Abstract

Electrostatic multipole interactions generate long-range Rydberg–Rydberg macrodimers. We calculate the adiabatic potentials of cesium $(nD_J)_2$ Rydberg macrodimers for principal quantum numbers n ranging from 56 to 62, for $J = 3/2$ and $5/2$, and for the allowed values of the conserved sum of the atomic angular-momentum components along the internuclear axis, M. For most combinations (n, M, J) exactly one binding potential exists, which should give rise to Rydberg macrodimer states. We study the dependence of the adiabatic potentials on the size of the two-body basis sets used in the calculation, and on the maximal order, $q_{\max}$, of the multipole terms included in the calculation. We determine the binding energies and lengths of the binding adiabatic potentials, investigate their scaling behaviors as a function of the effective principal quantum number, and discuss vibrational-state wave functions. We consider the applicability of the calculated potentials and excitation rates to an experimental scheme for preparing $(nD_J)_2$ Rydberg-atom macrodimers using two-color double-resonant photoassociation.

Keywords: Rydberg-atom macrodimers, electrostatic multipole interaction, adiabatic potentials

(Some figures may appear in colour only in the online journal)

1. Introduction

Rydberg atoms, highly excited states with large principal quantum number $n \gtrsim 10$, have been of interest in recent years due to their exaggerated properties [1], for example large sizes and electric-dipole transition matrix elements ($\sim n^2$), and strong long-range van der Waals interactions ($\sim n^{11}$). The strong interaction between Rydberg atoms results in an excitation blockade effect [2–6], which has led to a variety of interesting investigations and applications, including quantum logic gates [7, 8], single-photon sources [9, 10], single-photon transistor [11] and many-body systems and entanglement [12–14]. Including a wider class of electric-multipole interactions in the analysis, one finds adiabatic potentials with minima that may support bound Rydberg–Rydberg molecules [15–28]. These molecules are macrodimers, as their bond lengths scale approximately as $n^{2.5}$ and exceed the LeRoy radius, $\sim 4n^2$ (in atomic units), and can easily exceed 1 μm. Rydberg macrodimers have been first predicted theoretically for Rb $(nP)_2$ pair molecules [15]. Calculated potential energy curves for Rb $(n-1)P(n+1)P$ molecules were compared with experiments [16]. Similar work was performed on Rb $(n-1)DnS$ [19], Rb $(nS)_2$ and Rb $(nP)_2$ [21, 22], and Cs $(89D)_2$ macrodimers [17, 18] bound by long-range interaction. Rydberg macrodimers have been observed experimentally in cold atomic gases with cesium [20, 26–28], including $nD(n+2)D$ macrodimer [20], $nSn'F$ and $(nP)_2$ molecules for $22 \leqslant n \leqslant 32$ [26], $43P44S$ [27] molecules, and $(62D_J)_2$ Rydberg-atom macrodimers [28]. Certain Rydberg macrodimers are predicted to possess abundant vibrational states and exotic adiabatic potentials, which can be used to study vacuum fluctuations [29, 30], quench ultracold collisions [15], and measure correlations in quantum gases [20, 31].

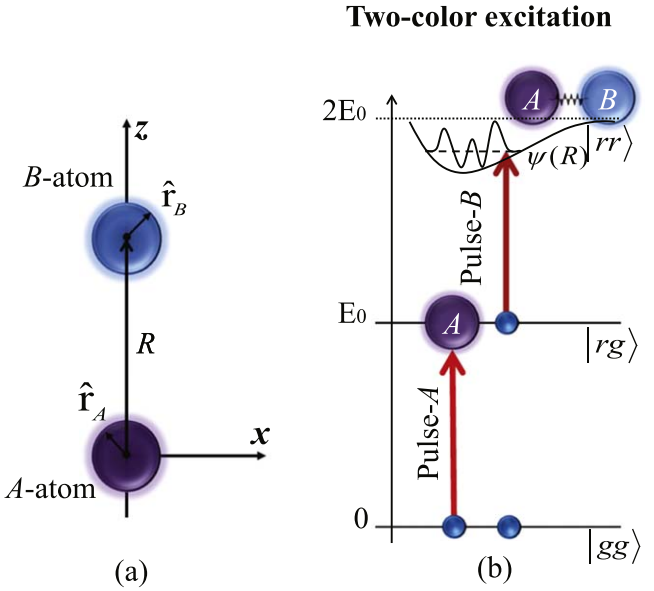

Figure 1. (a) Two-atom system. Rydberg atoms A and B, separated by $R > R_{LR}$, are placed on the z-axis, $\mathbf{r}_A$ and $\mathbf{r}_B$ are the relative positions of the Rydberg electrons in atoms A and B. (b) Level diagram and sketch of a vibrational wave-function for two-color double-resonant excitation of Rydberg-atom macrodimers. The pulse A resonantly excites seed Rydberg atoms (atom A). The frequency of pulse B is detuned relative to that of pulse A by an amount equal to the molecular binding energy.

The adiabatic potentials play an important role for the preparation of Rydberg macrodimers. The Rydberg macrodimers are identified by the assignment of photoassociation resonances to minima of the adiabatic potentials. In the present work, we investigate the adiabatic potentials of cesium Rydberg-atom pairs below the $(nD_J)_2$ $(n = 56 - 62)$ asymptotes, calculated considering the electrostatic multipole interaction between Rydberg-atom pairs. We explore the effect of the maximum interaction order on the potentials, for several basis sizes. We find that avoided crossings between adiabatic potentials affect the well shape, depending on the maximum multipole order considered and angular momentum quantum numbers. We discuss the bonding energies of $(nD_J)_2$ Rydberg dimers and the corresponding equilibrium internuclear distances as a function of n. We also calculate excitation rates for the case of a two-color excitation scheme used in recent experiments [28] and bound vibrational states. It is noted that the potential energy curves calculated in this work are not corrected for non-adiabatic effects that arise from the dependence of the electronic wavefunction on the internuclear separation.

2. Multipole interaction Hamitonian

For calculating the interaction of a Rydberg-atom pair, we consider two nD_J Rydberg atoms, denoted A and B, with an interatomic separation $\mathbf{R}$. To simplify the calculation, the quantization axis and $\mathbf{R}$ are both chosen along the z-axis, see figure 1(a). The relative positions of the Rydberg electrons are $\mathbf{r}_A$ and $\mathbf{r}_B$. The interatomic distance R is larger than the LeRoy radius [32], R_{LR}, i.e. the electronic wave functions do not overlap, and is small enough that radiation retardation effects [33] are not important. The Hamiltonian of the Rydberg-atom pair is written as:

$$\hat{H} = \hat{H}_A + \hat{H}_B + \hat{V}_{\rm int}, \tag{1}$$

where $\hat{H}_{A(B)}$ is the Hamiltonian of atom $A(B)$, and $\hat{V}_{\rm int}$ denotes the multipole interaction between the Rydberg-atom pair. $\hat{V}_{\rm int}$ is taken as [17, 26, 28, 34]

$$\hat{V}_{\rm int} = \sum_{q=2}^{q_{\rm max}} \frac{1}{R^{q+1}} \sum_{\substack{L_A=1 \\ L_B=q-L_A}}^{q_{\rm max}-1} \sum_{\Omega=-L_<}^{L_<} f_{AB\Omega}\, \hat{Q}_A \hat{Q}_B \tag{2}$$

$$f_{AB\Omega} = \frac{(-1)^{L_B}\,(L_A + L_B)!}{\sqrt{(L_A+\Omega)!(L_A-\Omega)!(L_B+\Omega)!(L_B-\Omega)!}}, \tag{3}$$

where $L_{A(B)}$ are the multipole orders of atoms $A(B)$, and the $L_<$ is the lesser of L_A and L_B. The sum over $q = L_A + L_B$ starts at 2, because the atoms are neutral and have no monopole moment, and is truncated at a maximal order $q_{\rm max}$. The factor $f_{AB\Omega}$ depends on L_A, L_B and the counting index Ω under the third sum. The $\hat{Q}_{A(B)}$ are expressed as:

$$\hat{Q}_A = \sqrt{\frac{4\pi}{2L_A+1}}\, \hat{r}_A^{L_A} Y_{L_A}^{\Omega}(\hat{\mathbf{r}}_A) \tag{4}$$

$$\hat{Q}_B = \sqrt{\frac{4\pi}{2L_B+1}}\, \hat{r}_B^{L_B} Y_{L_B}^{-\Omega}(\hat{\mathbf{r}}_B), \tag{5}$$

where the single-atom operators $\hat{\mathbf{r}}_A$ and $\hat{\mathbf{r}}_B$ are the relative positions of the Rydberg electrons in atoms A and B, the operators $\hat{Q}_{A(B)}$ include radial matrix elements, $\hat{r}_{A(B)}^{L_{A(B)}}$, and spherical harmonics that depend on the angular parts of the Rydberg-electron positions, $Y_{L_{A(B)}}^{\pm\Omega}(\hat{\mathbf{r}}_{A(B)})$. The radial wavefunctions of the atomic basis states $|n\ell Jm_j\rangle$ required to calculate the matrix elements of the $\hat{Q}_{A(B)}$ are obtained using an algorithm explained in [35] using model potentials from [36].

We diagonalize the Hamiltonian of the Rydberg-atom pair on a dense grid of the internuclear separation, R. The R range is 1.5–5.0 μm and the number of radial steps is 400. To improve the quality of the plots of the potential curves at small R, the radial steps are chosen equidistant in R^{-3}. Because of global azimuthal symmetry, the projection of the sum of the electronic angular momenta, $M = m_{JA} + m_{JB}$, is conserved. For the homonuclear diatomic system in this work, the inversion symmetry is employed to define symmetrized basis states [37], with $p = +1$ for even-parity states, $|\Psi_g\rangle$, and $p = -1$ for odd-parity states, $|\Psi_u\rangle$, that are not coupled by $\hat{V}_{\rm int}$. In order to obtain the adiabatic potential curves of the Rydberg-atom pair, the Hamiltonian matrix is separately diagonalized for even- and odd-parity states using various basis sizes (section 3) and values for the maximal multipole order, $q_{\rm max}$ (section 4), for a range of principal quantum numbers (section 5).

Other than in perturbative methods (see, for instance, [4]), in the present work the adiabatic potentials are obtained by exact diagonalization of the Rydberg-pair Hamiltonian,

equations (1)–(5) using large two-body basis sets and including binary interaction terms up to $q_{\max} = 6$. The adiabatic potentials, obtained by plotting the adiabatic energy values versus R, include perturbations due to $V_{\rm int}$ up to arbitrary order. In the case of accidental resonances (Förster resonances) between Rydberg pair states, $V_{\rm int}$ causes first-order contributions in the adiabatic potentials that asymptotically connect with the Förster-resonant pair states. The first-order shifts scale as $1/R^{q+1}$. For sufficiently non-degenerate Rydberg pair states, the leading coupling typically is a van-der-Waals interaction, i.e. a second-order interaction in $V_{\rm int}$ that scales as $1/R^{q+q'+2}$. The direct-diagonalization approach further accounts for $V_{\rm int}$-induced state mixing between pair states up to arbitrary order (within the utilized basis set). We also include the modifications of low-angular-momentum states, described by quantum defects, as well as fine structure. Due to these features, the direct-diagonalization approach is considerably more powerful than perturbative models of Rydberg pair interactions [4] in identifying adiabatic potentials with wells that lead to bound vibrational molecular states.

Numerical calculations of potential curves require a suitable basis set, which, together with $q_{\max}$, determines the number of (non-zero) interaction matrix elements used. The single-atom basis states are denoted $|n\ell J m_J\rangle$, and the corresponding Rydberg-atom pair basis states are denoted $|n_A \ell_A J_A m_{JA}\rangle \otimes |n_B \ell_B J_B m_{JB}\rangle$, with Rydberg atoms A and B. For the quantum defects of the atomic energies and the fine structure coupling constants [1, 38–40] in $\hat{H}_A$ and $\hat{H}_B$ we use published values. For high-n ($n = 56$–62 here), the atomic hyperfine coupling and the molecular rotation energy are orders of magnitude smaller than the molecular interaction energy $\hat{V}_{\rm int}$; they are therefore neglected. For the single-atom basis states, the range of effective principal quantum numbers is chosen as $\mathrm{int}(n_{\rm eff0}) - \Delta < n_{\rm eff} < \mathrm{int}(n_{\rm eff0}) + \Delta + 1$, where $n_{\rm eff0}$ is the effective quantum number of the Rydberg state of interest, $\mathrm{int}(n_{\rm eff0})$ denotes the integer part of $n_{\rm eff0}$, and Δ is a parameter for the principal quantum number range. Further, the single-atom orbital angular momentum space is restricted to $\ell \leqslant \ell_{\max}$ and $m_J \leqslant m_{J\max}$, for both atoms A and B. The energies of the two-body molecular states are measured relative to a state of interest, which in our case is of the type $nD_J nD_{J'}$, with J, $J' = 3/2$ or $5/2$. The two-body basis is then further truncated to two-body states with energy defects less than an upper limit of 27–37 GHz from the molecular state of interest, depending on n.

To estimate photo-association rates, we assume the atom sample is seeded with Rydberg atoms in state nD_J. We then calculate the photo-association rate for a second atom out of the state $6P_{3/2}$ using Fermi's Golden Rule. The second atom is located at internuclear distance R. The result is averaged over all angles, θ, of the internuclear axis relative to the frame defined by the excitation laser beam, and over all allowed values of the magnetic quantum numbers of the two atoms.

The calculation of excitation rates, which is presented in SI units, proceeds as follows. A symmetrized molecular state after diagonalization is

$$|\psi_{\rm mol}\rangle = \sum_{\lambda_A m_{JA} \lambda_B} c_{\lambda_A m_{JA} \lambda_B} (|\lambda_A m_{JA}\, \lambda_B m_{JB}\rangle - p(-1)^{\ell_A+\ell_B} |\lambda_B m_{JB}\, \lambda_A m_{JA}\rangle) \tag{6}$$

where λ_A stands for n_A, ℓ_A, J_A etc, and $c_{\lambda_A m_{JA} \lambda_B}$ denotes the (R-dependent) properly normalized wavefunction coefficients of the two-body basis states. The quantum numbers m_{JA} and m_{JB} are magnetic quantum numbers in the molecular frame of reference, where $m_{JB} = M - m_{JA}$. The excitation matrix element then is

$$V = \langle \psi_{\rm mol} | \hat{D}^{(J_e)}(\theta) \otimes \hat{D}(\theta) | \hat{\mathbf{I}} \otimes \hat{\Omega} | \lambda_e \omega_{Je}\, g \omega_{Jg} \rangle \tag{7}$$

with the (single-atom) seed Rydberg state $|\lambda_e \omega_{Je}\rangle = |nD_J,\, \omega_{Je}\rangle$ and launch state $|g\omega_{Jg}\rangle = |6P_{3/2},\, \omega_{Jg}\rangle$. The quantum numbers ω_{Je} and ω_{Jg} are magnetic quantum numbers in the frame defined by the excitation laser beams. The rotation operator $\hat{D}^{(J_e)}$ rotates the seed Rydberg atom from the laser frame into the molecular frame of reference. The operator $\hat{D} = \hat{D}^{(1/2)} \oplus \hat{D}^{(3/2)} \oplus \hat{D}^{(5/2)}$ rotates the optically excited Rydberg state $\hat{\Omega}|6P_{3/2},\, \omega_{Jg}\rangle$ from the laser into the molecular frame.

The laser excitation is described by

$$\hat{\Omega} = \frac{eE_0 \hat{\varepsilon} \cdot \hat{\mathbf{r}}}{2\hbar}, \tag{8}$$

where E_0 is the laser electric field amplitude and $e\hat{\mathbf{r}}$ the electric dipole operator, and $\hat{\varepsilon}$ a spherical laser polarization unit vector. The molecular excitation rate, ξ, is then given by

$$\xi = \left\langle \frac{2\pi}{\hbar} |V|^2 \rho \right\rangle_{\omega_{Je}, \omega_{Jg}, \theta}, \tag{9}$$

where $\langle * \rangle_{\omega_{Je}, \omega_{Jg}, \theta}$ denotes the average over the magnetic quantum numbers ω_{Je}, ω_{Jg}, and the angle θ. Further, ρ is the effective density of states. For a Gaussian laser frequency spectrum with full width at half maximum (FWHM) of $\delta\nu$, it is $\rho = \frac{2.35}{\sqrt{2\pi}\, h\, \delta\nu}$. The values of ξ describe the excitation rates, in s^{-1}, of the two-body state $|\lambda_e \omega_{Je}\, g \omega_{Jg}\rangle$ into Rydberg molecular states, $|\psi_{\rm mol}\rangle$, averaged over the allowed values of ω_{Je} and ω_{Jg}, and the angle θ (with angular weighting $\propto \sin(\theta)$). The rates ξ depend on R and are different for different adiabatic potentials.

3. Basis size

We calculate adiabatic potentials of $60D_{5/2}$-atom pairs with two different basis sizes for $M = 0$, $q_{\max} = 6$ and energy defect 30 GHz. One case is $54.9 < n_{\rm eff} < 60.1$ ($\Delta = 2.1$), and $\ell_{\max} = 4$, and J, $|m_J| \leqslant 4.5$, which results in a number of 3148 two-body basis states ($= 2 \times 1574$ symmetrized two-body states), see figure 2(a). The other case is for $53.9 < n_{\rm eff} < 61.1$ ($\Delta = 3.1$), and $\ell_{\max} = 5$, and J, $|m_J| \leqslant 5.5$, corresponding to a number of 7416 two-body basis states ($=2 \times 3708$ symmetrized two-body states). The calculated potential curves are shown in figure 2(b). For larger

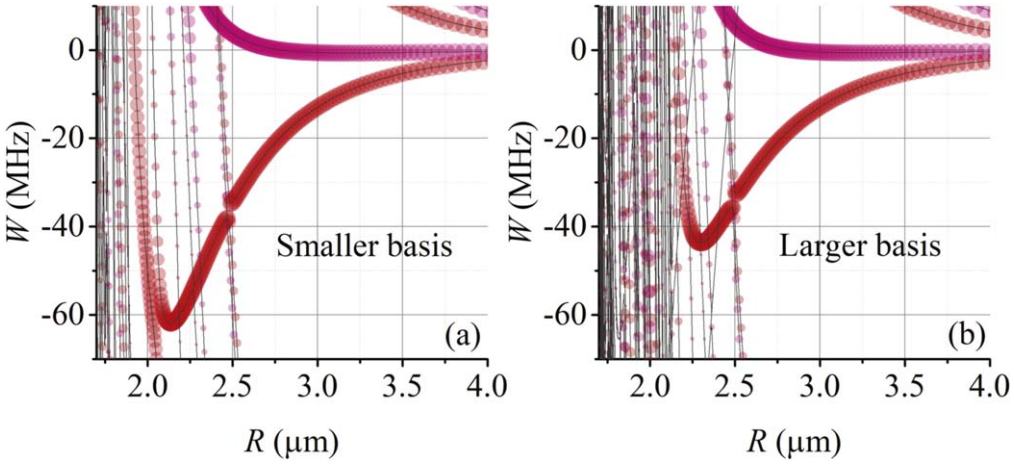

Figure 2. Calculations of adiabatic potential curves for cesium Rydberg-atom pairs, $(60D_{5/2})_2$, with $M = 0$ (black lines), $q_{\max} = 6$ and energy defect 30 GHz for a smaller (a) and a larger two-body basis size (b), with detailed truncation conditions explained in the text. Isotropic averages of laser excitation rates from the launch state $60D_{5/2}6P_{3/2}$, ξ, explained in the text, are proportional to the areas of the overlaid circles (red for symmetric, $p = +1$, and pink for anti-symmetric states, $p = -1$). The largest circle areas correspond to a rate of about 5×10^4 s^{-1} for a laser electric field of 10^4 V m^{-1}.

$|M|$-values, considered further below, the number of two-body states drops.

Both in figures 2(a) and (b), most potential curves with small excitation rates do not exhibit minima that could give rise to bound macrodimer states, except one binding potential. In the range $R \lesssim 2.1\ \mu$m, in figure 2(b), there are more potential curves, with some crossings, than in figure 2(a). However, these are not expected to produce observable effects, as there are no prominent wells associated with any of these steep, short-range potentials. In the range $R \gtrsim 2.1\ \mu$m, the differences between the small- and large-basis calculations are more subtle. Both cases have one potential curve with a wide minimum conducive to bound molecular states. Close inspection of figure 2(a) shows that the potential well with large oscillator strength exhibits a binding energy of $V_{\min} = 61.9$ MHz, at a bond length of $R_{\rm eq} = 2.13\ \mu$m. Increasing the basis size leads to some changes in these parameters. In figure 2(b), we find a binding energy that is 29% less than in figure 2(a), equivalent to a decrease of about 18.2 MHz, and a bond length that is 7% larger, corresponding to an increase of about 170 nm. These changes are attributed to level repulsion from additional levels in figure 2(b), which push the potential minimum up and out by some amount. The changes are large enough to become observable in an experiment.

In a third case, we have considered $(62D_{5/2})_2$ molecules with $M = 2$, for basis truncation parameters up to $54.9 \leqslant n_{\rm eff} \leqslant 64.9$, and $\ell_{\max} = 7$, and J, $|m_J| \leqslant 7.5$, with a maximum two-body energy defect 30 GHz (basis size up to 2×4857 symmetrized two-body states). We have seen that the potential minima with large oscillator strengths shift by amounts up to about 10 MHz, and that the increase in $|m_J|$-range has the largest effect.

In the present work, we cannot make a definite statement about whether convergence has been reached in figure 2(b), because at this time it is not practical for us to increase the two-body basis size far beyond about 10 000 with the codes (Fortran 77 and LAPACK) and work stations used. Additional work on convergence could possibly be performed at lower principal quantum numbers, where basis sizes are generally smaller, or by implementing the calculations on a high-performance computing platform. Despite the fact that the numerical calculations have not converged yet, they are suitable to demonstrate important features, such as the role of the maximum interaction order, $q_{\max}$, and trends of the potential well depths, $V_{\min}$, and bond lengths, $R_{\rm eq}$, versus principal quantum number n and angular-momentum M. In the following sections, we use the same quantum-number range as in figure 2(a), unless noted otherwise.

4. Dependence on multipole order

In equation (2), the electrostatic multipole interactions in $\hat{V}_{\rm int}$ scale as $1/R^{q+1}$ (outer sum in equation (2)). The multipole series proceeds through dipole–dipole (dd), dipole–quadrupole/quadrupole–dipole (dq/qd), dipole-octupole/octupole–dipole (do/od), quadrupole–quadrupole (qq), dipole–hexadecupole/hexadecupole–dipole (dh/hd) interactions, and so on, where the first (second) letter stands for atom $A(B)$. In our notation, the interaction series is terminated at the maximum order, $q_{\max}$. For example, for $q_{\max} = 2$ only the dd interaction is included. The case $q_{\max} = 3$ includes dd, dq and qd interactions, $q_{\max} = 4$ includes dd, do, od, dh, qq, and hd interactions, and so on. Since our calculation is based on numerical diagonalization of the Hamiltonian in equation (1), it includes the multipole interactions up to order $q_{\max}$ in a non-perturbative fashion, in all orders perturbation theory. For instance, for $q_{\max} = 2$ the second-order dd interaction, i.e. the usual van der Waals interaction, is automatically included.

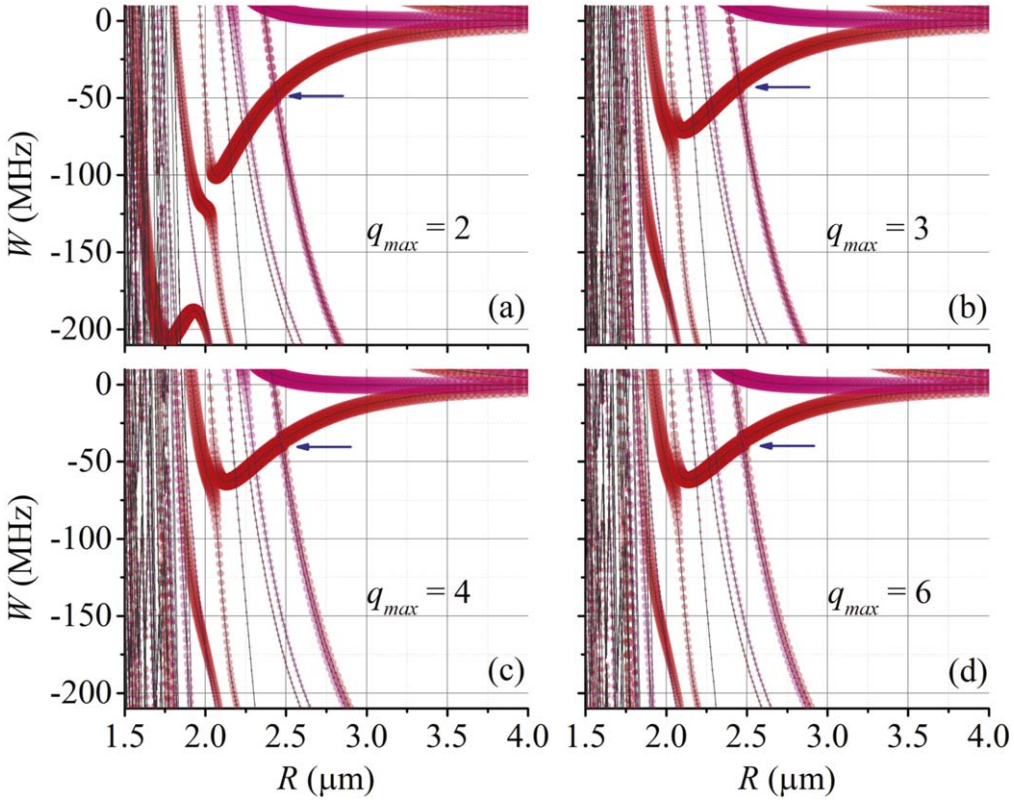

Figure 3. Adiabatic potential curves of $60D_{5/2}$ Rydberg-atom pairs with $M = 0$, the same quantum-number range as in figure 2(a), energy defect 30 GHz, and $q_{\max} = 2$(a), 3(b), 4(c) and 6(d). The higher-order terms push the potential well up and farther out. As $q_{\max}$ is increased from 2(a) to 6(d), the depth of the potential well diminishes by 39.0 MHz, and corresponding bond length increases by 0.07 μm. Further details are provided in table 1. The meaning of the red and pink symbols is analogous to figure 2. The arrows mark the positions of V_{cross} and R_{cross} for the outermost avoided crossing of the potential well.

To show how the value of $q_{\max}$ modifies the adiabatic potentials, in figure 3 we present the calculated adiabatic potential curves for the same quantum-number range as in figure 2(a), with $q_{\max} = 2$, 3, 4 and 6. Significant effects of interaction orders higher than dd can be seen near the potential minima. In figure 3(a), it is $q_{\max} = 2$, i.e. only dd-interactions are included, and the depth of the potential well that asymptotically approaches $W = 0$ is 100.9 MHz. As dq- and qd-interactions are added (figure 3(b)) the well depth decreases by 29.8 MHz. We also note that a second, inner well at -210 MHz and 1.8 μm, which is present at $q_{\max} = 2$, disappears upon inclusion of the $q = 3$ terms. These terms substantially increase the couplings of an apparent three-level avoided crossing near 2 μm. As a result, the inner well at -210 MHz is pushed down and disappears, and the outer well at -100.9 MHz is pushed up and reduced in depth. Including qq-, do- and od-interactions (figure 3(c)) reduces the depth of that well by an additional 7.9 MHz. The depths remains almost unchanged when $q_{\max}$ is increased further to 5 and 6. Between $q_{\max} = 4$ and 6 there are no significant changes in the shapes of the potential energy curves. To compare the effects of the interaction orders, $q_{\max}$, in table 1 we display the values $V_{\min}$ and R_{eq} for the potential well that asymptotically approaches $W = 0$, as well as V_{cross} and R_{cross} for the outermost avoided crossing of the corresponding adiabatic potential (marked by arrows in figure 3). From the study presented in figure 3, we have found that values of $q_{\max}$ of 5 or 6 are sufficient to model the adiabatic potentials.

Table 1. Binding energies, $V_{\min}$ in MHz, and corresponding equilibrium internuclear distances, R_{eq} in μm, versus $q_{\max}$ for Rydberg-atom pairs $(60D_{5/2})_2$ with $M = 0$. We also show the energies and positions of the outermost avoided crossing, marked with arrows, V_{cross} in MHz and R_{cross} in μm, respectively. Data are extracted from figure 3.

$q_{\max}$	$V_{\min}$	R_{eq}	V_{cross}	R_{cross}
2	−100.9	2.06	−46.3	2.44
3	−71.1	2.10	−39.5	2.46
4	−63.2	2.13	−35.2	2.49
5	−62.1	2.13	−34.9	2.49
6	−61.9	2.13	−34.8	2.49

Asymptotically, the leading term of a given potential curve depends on the detailed case. If the asymptotic Rydberg-atom state pair of the potential has a strong resonant coupling to another state pair via an accidental Förster resonance of multipole order $q \leqslant 4$, at large distances R the interaction energy scales as

Table 2. The binding energy, $V_{\min}$ in MHz, and corresponding equilibrium internuclear distance, $R_{\rm eq}$ in μm, of the adiabatic potentials for Rydberg-atom macrodimers, $(nD_J)_2$ ($n = 56 - 62$, $J = 5/2, 3/2$) and $M = 0, 1, 2, 3, 4$. The second column shows the energy-defect cutoffs, η, in GHz.

nD_J		$(nD_{5/2})_2$										$(nD_{3/2})_2$					
$M=$		0		1		2		3		4		0		1		2	
n	η	$V_{\min}$	$R_{\rm eq}$	$V_{\min}$	$R_{\rm eq}$	$V_{\min}$	$R_{\rm eq}$	$V_{\min}$	$R_{\rm eq}$	$V_{\min}$	$R_{\rm eq}$	$V_{\min}$	$R_{\rm eq}$	$V_{\min}$	$R_{\rm eq}$	$V_{\min}$	$R_{\rm eq}$
56	37	−79.2	1.80	−79.3	1.81	−78.2	1.78	−69.4	1.79	−61.3	1.64	−46.4	1.83	−40.1	1.83	−19.8	1.86
57	35	−74.2	1.88	−74.3	1.89	−73.2	1.86	−64.9	1.87	−57.0	1.71	−43.3	1.91	−37.3	1.92	−18.2	1.94
58	34	−70.8	1.96	−70.9	1.97	−70.0	1.94	−62.0	1.95	−55.4	1.78	−41.3	1.99	−35.8	1.99	−17.6	2.02
59	32	−65.8	2.05	−65.8	2.05	−64.8	2.03	−57.4	2.03	−50.3	1.86	−38.1	2.08	−32.7	2.08	−15.6	2.12
60	30	−61.9	2.13	−61.9	2.14	−60.9	2.11	−53.9	2.12	−47.0	1.95	−35.6	2.17	−30.5	2.17	−14.4	2.21
61	29	−59.0	2.22	−59.0	2.23	−58.1	2.20	−51.4	2.21	−45.1	2.02	−34.0	2.26	−29.1	2.26	−13.8	2.30
62	27	−54.8	2.31	−54.8	2.32	−53.8	2.29	−47.5	2.30	−40.8	2.11	−31.2	2.36	−26.6	2.36	−12.2	2.41

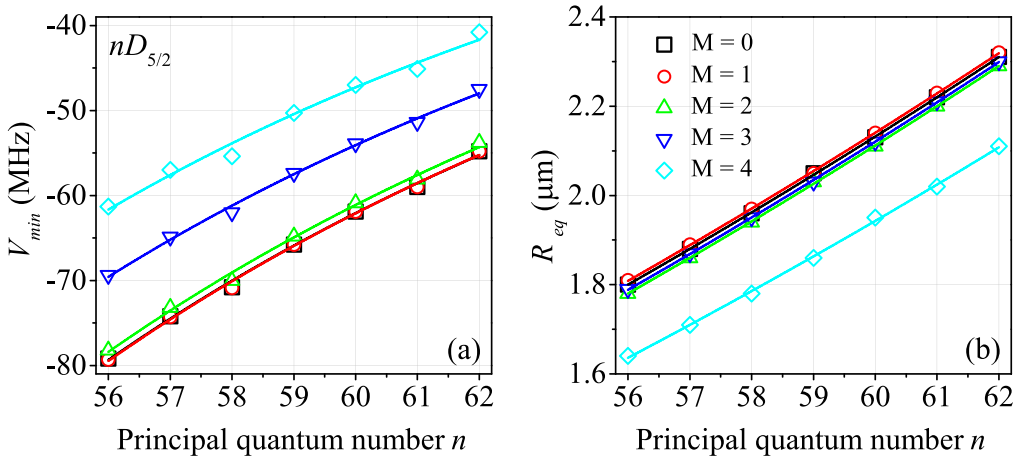

Figure 4. Calculations (symbols) of (a) binding energy, $V_{\min}$, and (b) corresponding bond length, $R_{\rm eq}$, of the adiabatic potential for cesium $(nD_{5/2})_2$ Rydberg macrodimers as a function of principal quantum number n. Solid lines show partial allometric fits, see text.

Table 3. The fitting parameters b from equation (6) for the binding energy, $b_{V_{\rm min}}$, and bond length, $b_{R_{\rm eq}}$.

nD_J	$(nD_{5/2})_2$		$(nD_{3/2})_2$	
M	$b_{V_{\rm min}}$	$b_{R_{\rm eq}}$	$b_{V_{\rm min}}$	$b_{R_{\rm eq}}$
0	-3.41 ± 0.07	2.35 ± 0.01	-3.65 ± 0.10	2.40 ± 0.02
1	-3.42 ± 0.07	2.34 ± 0.01	-3.77 ± 0.13	2.38 ± 0.03
2	-3.46 ± 0.09	2.37 ± 0.01	-4.38 ± 0.23	2.44 ± 0.03
3	-3.50 ± 0.09	2.36 ± 0.01	—	—
4	-3.69 ± 0.18	2.39 ± 0.03	—	—
average	-3.50 ± 0.11	2.36 ± 0.02	-3.93 ± 0.39	2.41 ± 0.03

$1/R^{q+1}$, due to the $R-$scaling in equation (2). If there is no low-order Förster resonance, at large distances the dipolar van der Waals interaction usually dominates (scaling $\propto 1/R^6$).

5. Dependence on principal quantum number

To determine the scaling behavior of the well depths and bond lengths with principal quantum number n, we have performed a series of calculations of the adiabatic potentials for nD_J Rydberg-atom pairs with $n = 56$ to 62, and $J = 3/2$ or $5/2$. The basis truncation parameters were $\Delta = 2.1$, $\ell \leqslant 4$, and J, $|m_J| \leqslant 4.5$, and maximal multipole order $q_{\max} = 6$. Further, we have scaled the maximum energy defect $\propto n_{\rm eff0}^{-3}$. The scaled maximum energy defects, denoted η in table 2, are consistent with the scaling of energy-level spacings between Rydberg states. With the scaling of the maximum energy defect, we keep the same types of pair states in all calculations. From the calculations, for each n we have extracted the adiabatic potentials below the $(nD_J)_2$ asymptotes that exhibit a binding potential well, which should give rise to Rydberg macrodimer states. For most combinations (n, M, J) exactly one such binding potential exists. For those, we determine the binding energies, $V_{\min}$, and corresponding bond lengths, $R_{\rm eq}$. These parameters are relevant to the preparation of Rydberg-atom macrodimers in experiments.

In figure 4, we present $V_{\min}$ and $R_{\rm eq}$ for $nD_{5/2}$-atom pairs. It is seen that the binding energy $|V_{\min}|$ decreases and bond length $R_{\rm eq}$ increases with increasing n. In the following, we explain the results for $M = 3$ in detail. The results for all M are then summarized in tables 2 and 3. We perform allometric-function fits of the well depth,

$$y = a(n - \delta_l)^b = a(n_{\rm eff0})^b, \tag{10}$$

where $\delta_l = 2.46$ is the D-state quantum defect, a and b are the fitting parameters, with b denoting the power scaling in $n_{\rm eff0}$. For $M = 3$, the fit parameters $b_{V_{\rm min}} = -3.50 \pm 0.09$, for the n-range of interest. The respective fit parameter for the bond length $R_{\rm eq}$, $b_{R_{\rm eq}} = 2.36 \pm 0.01$. To compare the fit results for the various cases, in table 2 we display the parameters $V_{\min}$ and $R_{\rm eq}$, and in table 3 we list the corresponding fit parameters b for all combinations (n, M, J). Averaging over M, it is $b_{V_{\rm min}}({\rm ave}) = -3.50$ and $b_{R_{\rm eq}}({\rm ave}) = 2.36$. Therefore, the potential depth $V_{\min}$ scales faster than the Kepler frequency (which scales as n^{-3}), and the bond length faster than the Rydberg-atom size (which scales as n^2).

To complete our study of cesium $(nD_J)_2$ Rydberg molecules, we have performed calculations on $(nD_{3/2})_2$ molecules analogous to results discussed above for $J = 5/2$. The data for $J = 3/2$ are shown in figure 5 and are included in tables 2 and 3. The potential depths and bond lengths are similar in the two cases of J. The bond length, $R_{\rm eq}$, exhibits similar scaling in the two cases, see table 3. There is a notable difference in the power scaling of $V_{\min}$; averaging over M it is

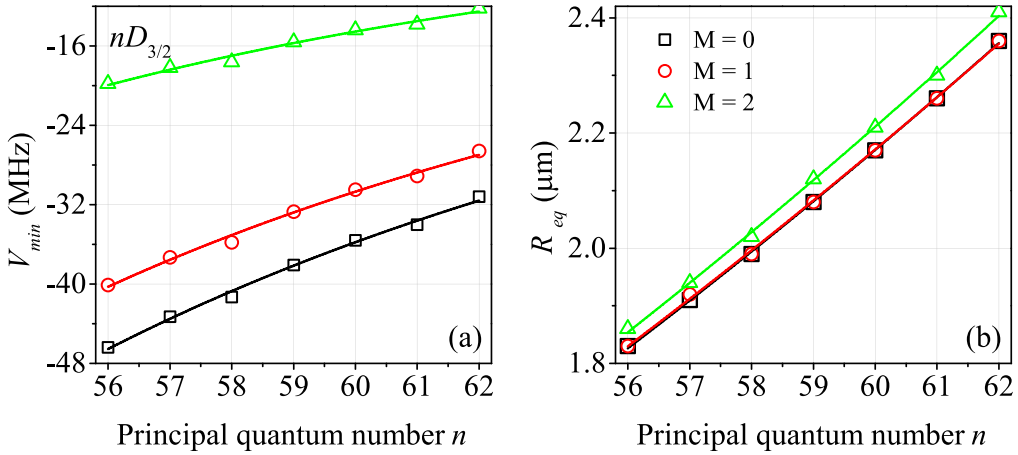

Figure 5. Calculations (symbols) of binding energy, $V_{\min}$, (a) and corresponding bond length, $R_{\rm eq}$, (b) and fits (solid lines) for $(nD_{3/2})_2$ Rydberg macrodimers. The figure is analogous to figure 4.

Table 4. Comparison of n-scalings of binding energies, $b_{V_{\min}}$, and bond lengths, $b_{\rm Re}$ for different types of molecules.

	Scaling	$b_{V_{\min}}$	$b_{R_{\rm eq}}$	Ref
Cs $(nD_{5/2})_2$	$\sim n_{\rm eff0}^{b}$	-3.50 ± 0.11	2.36 ± 0.02	this work
	$\sim n^{b}$	-3.65 ± 0.11	2.46 ± 0.02	
Cs $(nD_{3/2})_2$	$\sim n_{\rm eff0}^{b}$	-3.93 ± 0.39	2.41 ± 0.03	this work
	$\sim n^{b}$	-4.11 ± 0.41	2.51 ± 0.03	
Rb $(nS_{1/2})_2$	$\sim n^{b}$	-3	8/3	[22]
Rb $(nP_{3/2})_2$	$\sim n^{b}$	-3	8/3	[22]
Rb $nS_{1/2}n'S_{1/2}$	$\sim n^{b}$	-3	2.5	[21]

$V_{\min} \propto {n_{\rm eff0}}^{-3.93}$, the scaling is faster than for $J = 5/2$. We attribute this difference to the J-dependence of level repulsion effects from nearby adiabatic potentials. In table 4, we list a comparison of the n-scalings for different types of Rb Rydberg molecules for $V_{\min}$ and $R_{\rm eq}$. It is seen that for cesium $(nD_J)_2$ Rydberg molecules $V_{\min}$ exhibits a stronger n-scaling than for rubidium $(nS_{1/2})_2$, $(nP_{3/2})_2$ [22] and $nSn'S$ [21] Rydberg molecules, while $R_{\rm eq}$ scales slightly less strong.

In figure 6, we present bound states for the adiabatic potential of the $(56D_{5/2})_2$ $M = 3$ molecules in the energy range -70 to -60 MHz, marked with the a blue square in figure 6(a). It is visualized that Rydberg-atom molecules have abundant vibrational states with energy differences of about 1 MHz. The lowest vibrational energy gap is 822 kHz. Due to the anharmonicity of the potential, the gap sizes decrease quickly with increasing vibrational quantum number (see figure 6(b)).

6. Discussion and conclusion

The results presented in our work exhibit the role of the maximum interaction order, $q_{\max}$, as well as the trends in the potential well depths and bond lengths versus principal quantum number n and angular-momentum M. To explore the convergence of the results as a function of basis size further, we have studied convergence for the case $M = 3$ in a series of additional calculations. The results for the well depths and bond lengths are summarized in table 5. For the case $(60D_{5/2})_2$ it is seen that the potential minima keeps shifting up, as the basis size is increased. In the last round of basis size increase, from 5388 to 11 230 non-symmetrized states, the minimum shifts up by 9.2 MHz. While this is only about half of the change between basis sizes 2016 and 5388, one cannot claim convergence. Convergence of binding energies and bond lengths will likely require computations with even larger basis sizes, which may be performed on a HPC platform.

In recent experimental work, we have prepared $(nD_J)_2$ Rydberg–Rydberg macrodimers using a two-color double-resonant photoassociation method [28]. There, the level diagram and two-color excitation sketch displayed in figure 1(b) was applied. The first color (laser pulse A) resonantly excites Rydberg atom-A (seed atoms) from the ground state, and the second color (laser pulse B) is detuned relative to pulse A by an amount equal to the molecular binding energy. In this sequence, we excite B-Rydberg-atoms close to the A-atoms at a distance where a metastable Rydberg–Rydberg macrodimer exists. The calculations of potential energy curves and, in particular, of the excitation rates in the present work model this experimental scenario and provide guidance for future experiments.

In conclusion, we have numerically calculated the adiabatic potentials of cesium nD_J Rydberg-atom pairs generated by electrostatic multipole interactions between Rydberg atoms. We have used several basis sizes to obtain some insight into the basis size dependence of the results, and tested the dependence on the maximal multipole interaction order. We have determined the scaling behavior of the potential depth and bond length as a function of the effective principal quantum number, $n_{\rm eff0}$, and discussed our findings. We have found that it is important to include relatively far-detuned dipole-coupled pair states in the basis sets for the shape of the potential curves to converge. Achievement of overall convergence of the results as a function of basis size will require future work. We also note that, apart from convergence

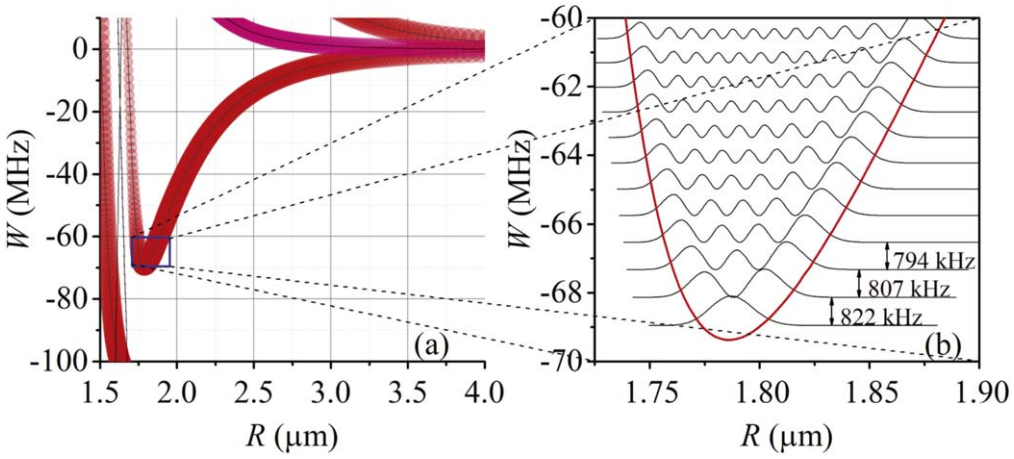

Figure 6. (a) Adiabatic potentials for $(56D_{5/2})_2$ with $M = 3$. The truncation parameters are the same as in figure 2(a), and $q_{max} = 6$. The meaning of the red and pink symbols is analogous to figure 2. (b) Calculation of the bound states in the range indicated by the blue square in (a).

Table 5. Binding energies, V_{min} in MHz, and corresponding equilibrium internuclear distances, R_{eq} in μm, of the adiabatic potentials of Rydberg-atom macrodimers, $(60D_{5/2})_2$ and $(62D_{5/2})_2$ for different basis sizes. The maximum interaction order is $q_{max} = 6$, and $M = 3$. The first six columns specify the atomic state, the range of the single-atom effective quantum number explained in section 2, Δ, the angular-momentum ranges, the cutoffs for the two-body energy defects, η in GHz, and the two-body basis sizes (before symmetrization).

State	Δ	ℓ_{max}	$(J, \lvert m_J\rvert)_{max}$	η	Basis size	V_{min}	R_{eq}
$60D_{5/2}$	2.1	4	4.5	30	2016	−53.9	2.12
	3.1	5	5.5		5388	−36.5	2.27
	4.1	6	6.5		11230	−27.3	2.43
$62D_{5/2}$	2.1	4	4.5	25	1712	−35.8	2.33
				27	2000	−47.5	2.29
				30	2140	−48.5	2.29

issues, the exact shapes of the potential energy curves are strongly dependent on the quantum defects. While these are very well known, they vary strongly between different atomic species and Rydberg-atom states. As seen in the related work cited (see introduction in section 1), there are other cases that produce potential energy curves with wells. Generally, every choice of atom and quantum-number combination requires a new calculation to determine the characteristics of that choice.

ORCID iDs

Jianming Zhao https://orcid.org/0000-0001-8420-9319

References

[1] Gallagher T F 1994 *Rydberg Atoms* (Cambridge: Cambridge University Press)
[2] Comparat D and Pillet P 2010 *J. Opt. Soc. Am.* B **27** A208
[3] Tong D, Farooqi S M, Stanojevic J, Krishnan S, Zhang Y P, Côté R, Eyler E E and Gould P L 2004 *Phys. Rev. Lett.* **93** 063001
[4] Singer K, Stanojevic J, Weidemüller M and Côté R 2005 *J. Phys.* B **38** S295
[5] Vogt T, Viteau M, Zhao J, Chotia A, Comparat D and Pillet P 2006 *Phys. Rev. Lett.* **97** 083003
[6] Vogt T, Viteau M, Chotia A, Zhao J, Comparat D and Pillet P 2007 *Phys. Rev. Lett.* **99** 073002
[7] Yang J, He X, Guo R, Xu P, Wang K, Sheng C, Liu M, Wang J, Derevianko A and Zhan M 2016 *Phys. Rev. Lett.* **117** 123201
[8] Isenhower L, Urban E, Zhang X L, Gill A T, Henage T, Johnson T A, Walker T G and Saffman M 2010 *Phys. Rev. Lett.* **104** 010503
[9] Dudin Y O and Kuzmich A 2012 *Science* **336** 887
[10] Peyronel T, Firstenberg O, Liang Q, Hofferberth S, Gorshkov A V, Pohl T, Lukin M D and Vuletić V 2012 *Nature* **488** 57
[11] Li W, Viscor D, Hofferberth S and Lesanovsky I 2014 *Phys. Rev. Lett.* **112** 243601
[12] Urban E, Johnson T A, Henage T, Isenhower L, Yavuz D D, Walker T G and Saffman M 2009 *Nat. Phys.* **5** 110
[13] Gaëtan A, Miroshnychenko Y, Wilk T, Chotia A, Viteau M, Comparat D, Pillet P, Browaeys A and Grangier P 2009 *Nat. Phys.* **5** 115
[14] Wilk T, Gaëtan A, Evellin C, Wolters J, Miroshnychenko Y, Grangier P and Browaeys A 2010 *Phys. Rev. Lett.* **104** 010502
[15] Boisseau C, Simbotin I and Côté R 2002 *Phys. Rev. Lett.* **88** 133004

[16] Stanojevic J, Côté R, Tong D, Farooqi S M, Eyler E E and Gould P L 2006 *Eur. Phys. J.* D **40** 3
[17] Schwettmann A, Crawford J, Overstreet K R and Shaffer J P 2006 *Phys. Rev.* A **74** 020701(R)
[18] Schwettmann A, Overstreet K R, Tallant J and Shaffer J P 2007 *J. Mod. Opt.* **54** 2551
[19] Stanojevic J, Côté R, Tong D, Eyler E E and Gould P L 2008 *Phys. Rev.* A **78** 052709
[20] Overstreet K R, Schwettmann A, Tallant J, Booth D and Shaffer J P 2009 *Nat. Phys.* **5** 581
[21] Samboy N, Stanojevic J and Côté R 2011 *Phys. Rev.* A **83** 050501(R)
[22] Samboy N and Côté R 2011 *J. Phys.* B **44** 184006
[23] Kiffner M, Park H, Li W and Gallagher T F 2012 *Phys. Rev.* A **86** 031401(R)
[24] Kiffner M, Li W and Jaksch D 2013 *Phys. Rev. Lett.* **110** 170402
[25] Samboy N and Côté R 2013 *Phys. Rev.* A **87** 032512
[26] Deiglmayr J, Saßmannshausen H, Pillet P and Merkt F 2014 *Phys. Rev. Lett.* **113** 193001
[27] Saßmannshausen H and Deiglmayr J 2016 *Phys. Rev. Lett.* **117** 083401
[28] Han X, Bai S, Jiao Y, Hao L, Xue Y, Zhao J, Jia S and Raithel G 2018 *Phys. Rev.* A **97** 031403(R)
[29] Ford L H and Roman T A 2011 *Ann. Phys.* **326** 2294
[30] Menezes G and Svaiter N F 2015 *Phys. Rev.* A **92** 062131
[31] Stecker M, Schefzyk H, Fortágh J and Günther A 2017 *New J. Phys.* **19** 043020
[32] Le Roy R J 1974 *Can. J. Phys.* **52** 246
[33] Casimir H B G 1946 *Nature* **158** 787
[34] Deiglmayr J 2016 *Phys. Scr.* **91** 104007
[35] Reinhard A, Cubel Liebisch T, Knuffman B and Raithel G 2007 *Phys. Rev.* A **75** 032712
[36] Marinescu M, Sadeghpour H R and Dalgarno A 1994 *Phys. Rev.* A **49** 982
[37] Weber S, Tresp C, Menke H, Urvoy A, Firstenberg O, Brüchler H P and Hofferberth S 2017 *J. Phys.* B **50** 133001
[38] Seaton M J 1983 *Rep. Prog. Phys.* **46** 167
[39] Goy P, Raimond J M, Vitrant G and Haroche S 1982 *Phys. Rev.* A **26** 2733
[40] Weber K H and Sansonetti C J 1987 *Phys. Rev.* A **35** 4650